Development and Characterization of a Murine Moderate Controlled Cortical Impact Model of Traumatic Brain Injury

A Thesis Submitted to the Faculty of the University of Minnesota By

Olivia Linn Erlanson

In Partial Fulfillment of the Requirements for the Degree of Master of Science

Advisor: Walter Low, PhD

August, 2025

Acknowledgements

I would like to thank my advisor Walter Low, PhD for his constant encouragement and support of my journey as a scientist. I must also thank my lab mates for their contributions to my thesis project and more importantly, for their love and friendship. To my committee members, Andrew Grande, MD and R. Scott McIvor, PhD, thank you for supporting me and always challenging me to be the best scientist I can be. Lastly, thank you to my loving family and friends for always believing in me, your love and support means more than words can describe.

Abstract

Traumatic brain injury (TBI) is a leading cause of long-term disability, with complex region-specific consequences that demand precise modeling. This study characterizes the structural, cellular, and functional impact of moderate anterior TBI in mice using a controlled cortical impact (CCI) model. Lesion volumes, quantified using 3D ultrasound, were consistent (2.4-2.7mm3). Histology revealed robust gliosis in perilesional regions with widespread microglial (Iba1) and astrocytic (GFAP) activation, extending bilaterally into the cortex and hippocampus while sparing the amygdala. Behaviorally, mice exhibited significant motor and spatial memory deficits, aligning with sensorimotor and hippocampal injury, while fear-conditioned learning remained intact, consistent with preserved amygdalar function. Together, these findings demonstrate that anterior CCI produces reproducible, regionally selective lesions that drive motor and hippocampal-dependent memory impairments while sparing fear-associated circuitry. Integration of 3D ultrasound with behavioral and histological analyses links lesion topography and neuroinflammation to functional outcomes, enhancing the translational relevance of this model.

Table of Contents

List of Figures

List of Tables

Chapter 1: Introduction

Traumatic brain injury (TBI) is the leading cause of death and disability among all trauma related injuries worldwide and is thus, a major global public health concern.[1] The global incidence of TBI is estimated at around 64-74 million people annually. Of these cases, around 55.9 million people per year will suffer from a mild TBI, while 5.48 million people per year will suffer from severe TBI.[2] In humans, TBI severity is commonly classified by the Glasgow Coma Scale (GCS), which is a 3- to 15- point scale utilized to assess a patient's neurologic function and level of consciousness.[3] Conversely, preclinical animal models of TBI have no standardized method for defining injury severity.[4] Thus, there is a critical need for a preclinical animal model of TBI with clearly defined injury severity classification parameters.

TBI has two injury phases: primary injury and secondary injury. Primary injury occurs at the moment of impact and causes immediate damage to the brain including axonal shearing and tissue degeneration. Secondary injury occurs over time as a result of cascades of cellular and metabolic events that lead to glial, endothelial, and neuronal cell death as well as white matter degeneration.[5,6] TBI also introduces a wide variety of chronic neurobehavioral sequelae, including motor coordination impairments and cognitive deficits, that play a role in the development of behavioral disorders and post-traumatic neurodegeneration.[7] Depending on the severity of the injury, the associated physical and neurobehavioral responses may improve or worsen over time. These effects are

likely to be significantly worsened in moderate to severe TBI cases, leading to devastating conditions for the people affected that can lead to difficulty returning to their jobs and reduced quality of life.[7] According to the CDC, ~50% of individuals who have survived moderate to severe TBI can experience this progressive decline in their quality of life or face a significant risk of mortality within five years of injury in spite of treatment.[8]

After TBI, the secondary injury phase triggers a cascade of inflammatory responses, mainly caused neuroinflammatory activation. Proinflammatory signals from severed neurons promote the widespread activation of microglia and astrocytes which in turn release proinflammatory and anti-inflammatory mediators.[9-11] Microglia and astrocytes, the resident immune cells in the central nervous system, shape and maintain their local environment by regulating the formation of synapses, providing support for neural plasticity, blood-brain barrier maintenance, eradicating cellular and molecular debris through phagocytosis, and releasing inflammatory molecules.[12,13] Chronically activated microglia and astrocytes are associated with a pro-inflammatory phenotype which damages the healthy neural tissue surrounding the local environment and in turn, causes progressive neuronal loss and further tissue damage.[13-16] This long term activation is considered to be a key factor in the exacerbation of debilitating neurological consequences following TBI, including the development of neurodegenerative diseases like Alzheimer’s and Parkinson's.[17-19] Therefore, detecting activated microglia and astrocytes and the subsequent alterations they

induce in the CNS along with the ability to guide their acute and long-term response to TBI is crucial for early detection and the development of therapeutic approaches.

There are currently no established therapies for chronic TBI. However, supportive therapies such as surgical intervention, rehabilitation, and medications to treat TBI symptoms are currently used to maintain quality of life.[20] Existing TBI treatments fail to provide neuroprotective and/or neurorestorative options that prevent patients from experiencing a lifetime of physical, emotional, cognitive, and behavioral changes with underlying chronic neurological deficits. Several promising therapeutic candidates have been proposed in pre-clinical TBI models to combat these limitations, though none have been shown to provide clinical effectiveness.[21,22] This failure to translate therapeutics from the preclinical to the clinical setting may, in part, arise from the difficulty of creating an animal model that fully recapitulates every aspect of TBI seen in humans.[6] Yet, animal models remain crucial for studying TBI as they allow for the interrogation of injury mechanisms, novel therapeutic candidates, neurobehavioral changes, and pathophysiological aspects of TBI that are otherwise not able to be studied in humans.[6,23]

There are several available animal models of TBI currently developed, including fluid percussion injury (FPI), weight-drop, and controlled cortical impact (CCI). While all of these models reproduce key features seen in human TBI such as behavioral and histological changes, the FPI and weight-drop models are

associated with high mortality.[6] Additionally, weight-drop models are subject to a high degree of variability and lack reproducibility.[6] The CCI model, however, is easily reproducible, creates nearly identical injuries across groups, and allows for easy control of mechanical factors like velocity, dwell time, and depth of impact, thus making it a more suitable option for studying moderate TBI.[6,24]

Though numerous studies of TBI using the CCI model are published, several inconsistencies remain that stem from differences in injury parameters/severity, behavioral task parameters, and the timing of injury evaluation post injury.[25] Thus, a model of moderate traumatic brain injury with clearly defined post injury evaluation, behavioral analysis parameters, and histological evaluation is needed. In this study, we developed a murine CCI model of moderate traumatic brain injury targeting the anterior sensory-motor cortices of the brain and characterized its effects on behavioral and histological outcomes following injury. The goal of this research is to determine what behavioral and histological changes are associated with moderate TBI in the anterior cortical site of injury. We hypothesize that we will see behavioral deficits in locomotor and somatosensory functions. Since these areas of the cortex also interact with other regions of the brain, it is a possibility that other behaviors will also be affected by TBI in the anterior cortical coordinates. The behavioral tests employed in this study will delineate the relationship between TBI in this lesion site with behaviors that are also mediated by other regions of the brain. The histopathological analyses will enable us to study the relationship between long

term behavioral deficits and possible chronic inflammation via the activation of microglial cells and astrocytes.

Chapter 2: Materials and Methods

2.1 Animals:

7–9-week-old male and female C57BL/6J mice (n=20, 10 males and 10 females) were obtained from the Jackson Laboratory and maintained at the University of Minnesota Research Animal Resources facilities under specific pathogen-free conditions. Animal care and procedures were performed according to the University of Minnesota Institutional Animal Care and Use Committee (IACUC). Mice were housed under a reversed light cycle for one week prior to entering the experimental pipeline.

2.2 Controlled Cortical Impact:

To induce TBI via CCI, mice (n=12, 6 males and 6 females) were anesthetized with 1.5-5% isoflurane. Following anesthetization, mice were secured to a stereotaxic frame where lubricant was applied to the eyes, and Nair^{tm} was applied to the head (~ 1 minute) and removed with betadine and alcohol wipes. After deep anesthesia was achieved (checked via toe pinch method), a craniotomy was performed over the motor and sensory cortical areas of the brain. The exposed dura was impacted using an Impact OneTM Stereotaxic Impactor device (Model 39463920 Leica Biosystems; Buffalo Grove, IL) at the coordinates relative to Bregma: AP = 0, ML = 1.5 mm lateral (right hemisphere), and DV = - 1.0 mm. A probe tip diameter of 2.0 mm was used to penetrate the brain parenchyma with a velocity of 6.0 m/s, and a dwell time of 100 ms. To ensure the consistency of TBI between animals, an electronic contact sensor and

surgical loops were utilized to confirm contact of the impactor tip to the brain surface. Following impact, the incision was sutured closed, and mice were injected with extended-release Buprenorphine (3.25 mg/kg, Ethiqa XR). Finally, mice were removed from the anesthesia and stereotaxic frame and allowed to recover in a cage with a heating pad underneath. The body temperature of the mice was maintained at 37°C throughout the entire procedure.

2.3 Behavior Testing:

All behavioral tests were performed at the UMN during the animals' active phase (dark cycle). Mice underwent behavior testing at 1-, 6-, 13-, 20-, and 27-days post injury (DPI) for beam walk, 1-, 6-, and 27 DPI for rotarod, 34-38 DPI for Barnes maze, and 41-42 DPI for delay fear conditioning. All animals were given 30 minutes to acclimate to their surroundings before beginning behavior testing. ANYmaze tracking software (Stoelting Co.) was used for all behavioral assessments.

2.3.1 Beam Walk:

Beam walk was used to assess individual limb function. Prior to performing this task, mice were trained to walk on a 6-mm-wide beam for three days prior to injury. Each animal was given 3 trials per day to traverse the beam in 60 seconds or less. The number of foot faults accrued over 50 steps were counted for the left hind limb of each mouse. Baseline results were recorded as the average number of total foot faults over the three days of training.

2.3.2 Rotarod:

Rotarod was utilized to assess fine balance and motor coordination in mice. All mice were trained for 3 days prior to injury. Each animal was given 3 trials per day and at least two minutes of recovery between each trial. The test was performed over a period of five minutes, with an acceleration of 4.0-60.0 RPM and a five second delay between accelerations. Results were recorded as the time it takes to fall off the rotating rod (latency to fall).

2.3.3 Barnes Maze:

Barnes maze was utilized to evaluate the spatial memory of mice. Here, a 20-hole maze platform containing a singular hidden escape box with a small ramp was placed in the center of a brightly-lit room (300-1000 lux). Posters containing colorful geometric shapes were placed on the walls around the room to act as spatial cues and kept consistent in location throughout testing. Animals were tested in groups of 5 and given a 10-15 minute inter trial interval (ITI) between each trial. The mice were trained over a period of four days and given 4 trials per day. On the fifth day, mice were subjected to a singular 90s duration probe test where the escape hole was removed and covered. For each trial, the mouse was placed in the center of the maze under a bucket for 10-15 seconds. The bucket was then removed, and the trial was started. Mice were then allowed to explore the maze for a maximum of 180s. If the mouse failed to locate the escape box within the allotted time, it was gently guided to the escape hole. If the animal escaped early, the trial was stopped, and the animal was allowed to rest

in the escape hole for 30-60s with the bucket over the top. To control for odor cues and scent tracking, the maze was rotated 90° between groups and cleaned with ethanol after each trial, with the escape box location kept consistent during rotation. Any-Maze video software (Stoelting Co.) was utilized to record the total number of holes visited, total distance traveled, and the latency to escape for each trial as well as the duration spent in each zone during the probe test. Spatial search strategies were analyzed using the BUNS (Barnes maze unbiased strategy) classification tool.[26] Possible search strategies range from non-spatial to highly spatial: (1) random search indicates the inability of the animal to locate the escape hole using spatial cues; (2) serial search indicates that the animal located the escape hole by traveling from one hole to the next rather than using spatial cues; (3) focused search indicates the animal was able to scan a localized area surrounding the escape hole; (4) long-correction, where the animal makes a major correction in trajectory to reach the escape hole; (5) corrected, where the animal makes a slight correction in their path to the target hole; and (6) direct,

where the mouse identifies the escape hole location using the shortest possible trajectory.[26]

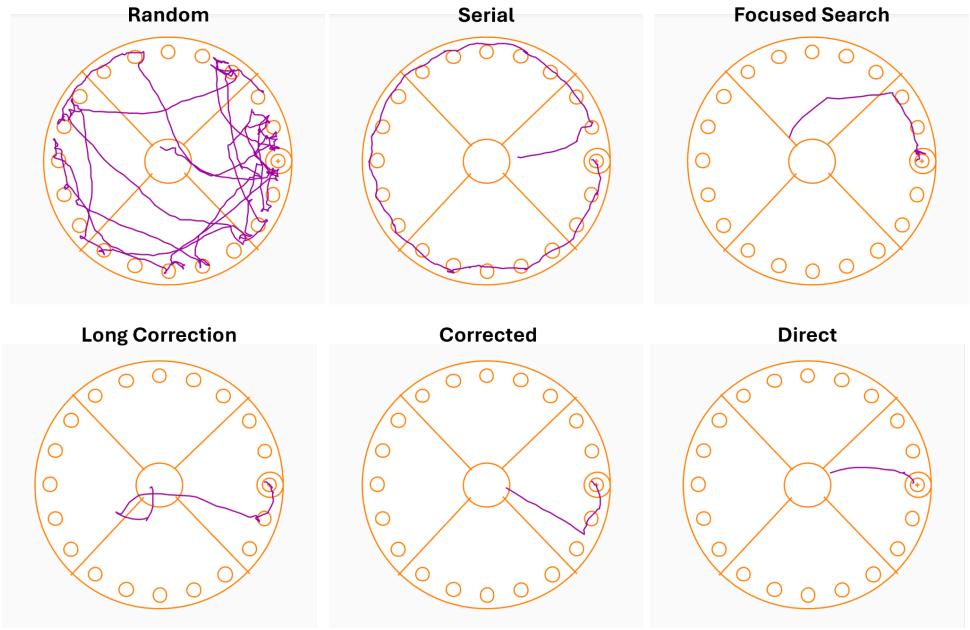

Figure 1. Examples of Search Strategies. Search strategies range from nonspatial (top-left) to highly spatial (bottom-right).

2.3.4 Fear Conditioning:

Delay fear conditioning was utilized to evaluate associative learning and memory formation. On day 1 (conditioning phase), animals were placed in a sound attenuated fear conditioning chamber (Ugo Basile) containing metal grate flooring and walls, with Simple Green (1:2 dilution) lightly sprayed in the bottom metal tray as an odor cue. Here, mice were tested for a total duration of 9 minutes, which included a 2-minute habituation period followed by 5 15 second tone/light/shock pairings (0.7mA) spaced 60 seconds apart. On day 2, context dependent memory was tested by returning the mice to identical chambers 24 hours after the training session, where mice spent 3 minutes in the testing chamber with no cues, only 1:2 Simple Green odor. Cued memory was then

tested by placing the animals in their prospective chambers 1-2 hours after the context test. Here, the chamber interiors were replaced with white plastic flooring and curved walls, and the Simple Green olfactory cue was replaced with 0.5% vanilla spray. Mice spent 6 minutes in the testing chambers where the final two minutes were paired with light and tone cues. Time spent freezing in the chambers was recorded and analyzed using ANY-maze software (Stoelting Co.) for each test and evaluated as % of time spent freezing in each respective testing condition.

2.4 Tissue Processing:

2.4.1 Euthanasia and Tissue Fixation:

Mice were anesthetized with isoflurane and euthanized through trans-cardiac perfusion with PBS and 4% Paraformaldehyde (PFA), then decapitated. Following decapitation, their brains were removed from the skulls and placed in 4% PFA for 24 hours at 4°C. The next day, brains were transferred to 70% ethanol for long term storage.

2.4.2 3D Ultrasound:

All TBI brains were scanned using a Vevo 2100 Imaging System with a MS400 transducer attached to a 3D acquisition motor via stereotaxic arm. Brains were removed from 70% ethanol, positioned in a center well culture dish containing ultrasound gel for stability, then submerged in water. The transducer, via the stereotaxic arm, was then positioned at the center of the brain and set to acquire a range of +/- 7mm with a step size of 0.1mm.

2.4.3 Histology:

Mouse brains were processed via formalin-fixed paraffin-embedding (FFPE), where the brains were fixed in formalin, dehydrated in a graded series of ethanol solutions, cleared with xylene, and embedded in paraffin blocks. Paraffin brain blocks were then sectioned coronally into six-micrometer thick slices using a Leica RM2125 microtome (Leica Biosystems) and collected on SuperFrost Plus® slides (Thermo Fisher Scientific Inc.). For immunofluorescence staining, sections were first deparaffinized in xylene, rehydrated in a series of ethanol solutions (100%, 95%, 70%, and 50%), then rinsed in deionized water. Antigen retrieval was then performed by steaming the sections in boiling 10mM citrate buffer (pH 6.0) for 20 minutes. Following antigen retrieval, sections were rinsed in PBS for 15 minutes, permeabilized with PBST (0.3% Triton X-100) for 30 min, and blocked with 5% donkey serum for 1hr. Sections were then incubated with primary antibodies against Iba-1 (1:1000, 013-27691, FUJIFILM Irvine Scientific) and GFAP (1:1000, PA1-10004, Invitrogen) overnight at 4 °C in 5% donkey serum blocking solution. Next, sections were washed 3x5 min with PBST (0.1% Triton X-100), then incubated with DAPI (1:1000), Donkey anti-Rabbit Alexa Fluor 647 (1:1000, A-31573), and Donkey anti-Chicken Alexa Fluor 488 (1:1000, A-78948) in 5% donkey serum for 1 hour. Lastly, sections were rinsed 3x5 min with PBS, mounted using Fluoromount-G™ (00-4958-02), and imaged using a Leica DMI6000 B microscope at 10X and 40X magnification.

2.5 Tissue Quantification:

2.5.1 Lesion Volume Analysis and Mapping:

To quantify TBI lesion volumes, 3D Slicer was used on the previously acquired ultrasound scans.[27] Images from the scans were spaced at values of 0.0890 mm (165), 0.0189 mm (1204), and 0.0204 mm (988). First, Segment Editor was used to segment the images into two distinct regions: Segment 1 to depict the outline of the brain and segment 2 to depict the missing TBI lesion. Here, Segments 1 and 2 were highlighted using the paintbrush tool every 10 slides. Next, the 'Grow from seeds' tool was utilized to carry out the initial segmentation. Both segments were then smoothed using a factor of 0.2-0.3. Following smoothing, segment 2 was cropped so that only the TBI lesion was included. Slides were then manually trimmed so that the shape of both sides of the brain matched. The segmentation values were then calculated using the 'Segment Statistics' tool and exported. Lastly, the 3D lesion ultrasounds were mapped to the Allen Brain and Annotation Atlas to determine the average volume lost per brain region as previously described.[42]

2.5.2 Cell Quantification:

To quantify the number of activated microglia and astrocytes present in the brain, QuPath software was utilized.[28] First, images (10x) were imported into the program and set to the image type 'fluorescence'. Annotation areas were then made to identify a small region of inactivated cells using the rectangle tool. Next, the 'cell detection' function was utilized to calculate the number of cells present

as well as the area of the detected cells. Cell area measurements were then exported to Excel, where the average cell area, standard deviation, and size threshold for activated cells were calculated. Next, annotations of the ipsilateral and contralateral cortices and hippocampi were made, and the cell detection step was repeated with the same settings. Lastly, we calculated the percentage of activated cells present by determining how many cells exceeded the threshold, and thus, the ratio of activated cells to total cells.

2.6 Statistical Analysis:

All quantitative values were expressed as mean ± standard error mean (SEM). Statistical analyses were performed using GraphPad Prism 10.4.1. One-way ANOVA (analysis of variance) and Two-way ANOVA with Tukey's HSD test were used to identify and assess significant differences between TBI and WT animals. A two-tailed unpaired t-test was used to determine the significance between groups for lesion volume analysis. A p-value of <0.05 was considered to be significant.

Chapter 3: Results

3.1 Beam Walk:

Individual limb function and fine motor coordination were assessed using beam walk. Here, mice underwent training for 3 consecutive days prior to CCI injury and were tested on 1-, 6-, 13-, 20-, and 27 DPI. The number of foot faults accrued over 50 steps were counted for the left hind limb of each mouse. Prior to injury (during baseline acquisition), all mice performed similarly with no significant differences in foot faults seen (Fig. 2). Total foot faults were significantly increased in TBI males and females as compared to WT males and females at 1 DPI ($p<0.0001$ and $p=0.0016$, respectively). This trend was also seen at 13-, 20-, and 27 DPI (Fig. 2). Interestingly, TBI females performed fewer foot faults than TBI males consistently over time. This trend was only significant at 20 DPI, where TBI females had an average of 13.8 (±2) FF and TBI males had an average of 32 (±4.9) FF ($p=0.0449$, Fig. 2). Over time, the mean number of foot faults between the WT males and WT females did not differ significantly.

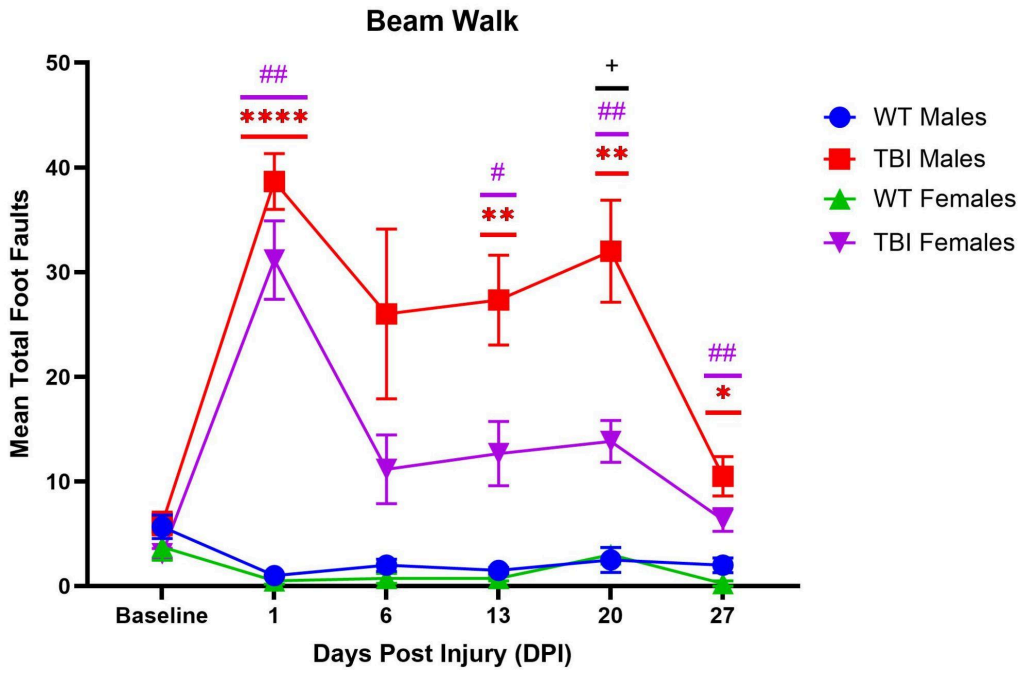

Figure 2. Beam Walk Results. Significantly increased foot faults were seen for TBI male and TBI female mice at 1 DPI *(**** p<0.0001, ## p=0.0016),* 13 DP*I (** p=0.0068, # p=0.0413),* 20 DPI *(** p=0.0055, ## p=0.0083, + p<0.05),* and 27 DPI *(* p=0.0191, ## p=0.0080).* Values are mean ± SEM. Statistical analysis by two-way ANOVA with Tukey HSD post-test. Asterisks (*) indicate significance between TBI and WT males, pound signs (#) indicate significance between TBI and WT females, plus signs (+) indicate significance between TBI males and females.

3.2 Rotarod:

Fine balance and motor coordination were evaluated utilizing the rotarod behavioral test on days 1-, 6-, and 27 DPI (see Materials and Methods). Similar to the beam walk, TBI male and female mice displayed significantly decreased latencies to fall when compared to WT male and female mice at 1 DPI (*p≤0.0034*, Fig. 3A and 3B). Significant differences in fall latencies were also seen between TBI and WT female mice at 6 DPI (*p=0.0285,* Fig. 3B). At 27 DPI, TBI females had an average fall latency of 87.7 (±7.3) while WT females had an average fall

latency of 117.8 (±14.1), though not significant (Fig. 3B). At 6 DPI and 27 DPI, WT males and TBI males showed similar latencies to fall, and thus did not differ significantly (Fig. 3A).

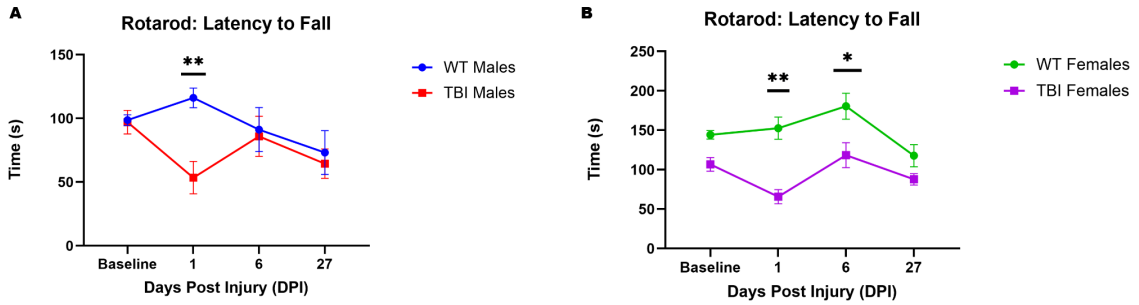

Figure 3. Rotarod Results. (A) TBI male mice spent significantly less time on the rotating apparatus at 1 DPI (**p=0.0033)*. (B) TBI female mice spent significantly less time on the rotating apparatus at 1 DPI and 6 DPI (*** p=0.0028*, ** p=0.0285*). Values are mean ± SEM. Statistical analysis by two-way ANOVA with Tukey HSD post-test.

3.3 Barnes maze:

Spatial learning and working reference memory were interrogated via the Barnes maze behavioral test (see Materials and Methods).

3.3.1 Total Latency to Escape:

Latency to escape (i.e. the time it takes for the mouse to find and enter the escape hole) improved over time for all groups, indicative of learning. Two-way ANOVA with Tukey's HSD post-test revealed that escape latencies did not differ significantly between WT and TBI males over time, while TBI females took significantly longer to escape than WT females on the first day of training (*p=0.0462,* Fig. 4A and 4B). Although the initial two-tailed two-way ANOVA did not yield a significant group × time interaction (*p=0.0949*), a follow-up one-tailed analysis—based on the A Priori hypothesis that TBI animals would demonstrate

slower learning relative to WT animals—revealed a significant group × time interaction between TBI and WT females (*p=0.047,* Fig. 4B). Conversely, no significant group x time interaction was seen between TBI and WT males (Fig. 4A).

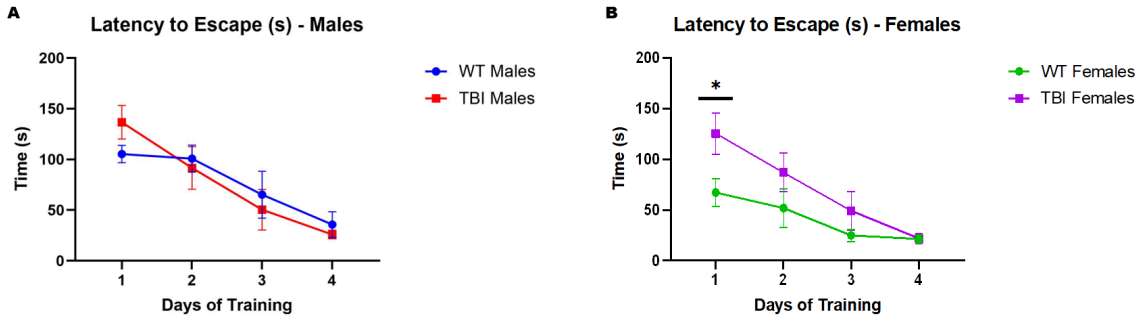

Figure 4. Latency to Enter Escape Hole. (A) Escape latencies of WT and TBI males over four days of training. No significant differences were observed (*p>0.05*). (B) Escape latencies of WT and TBI females over four days of training. Significant differences were seen on the first day of training (**p=0.0462*). Additionally, a significant group x time interaction was observed (*p=0.047*). Values are mean ± SEM. Significance determined by two-way ANOVA with Tukey HSD post-test.

3.3.2 Total Errors Made:

The total numbers of errors made (e.g. the number of head pokes made into holes other than the escape hole) decreased over the four days of training for all experimental groups, indicative of learning. No significant differences in the number of errors made were seen between TBI animals and WT animals over time (Fig. 5A and 5B).

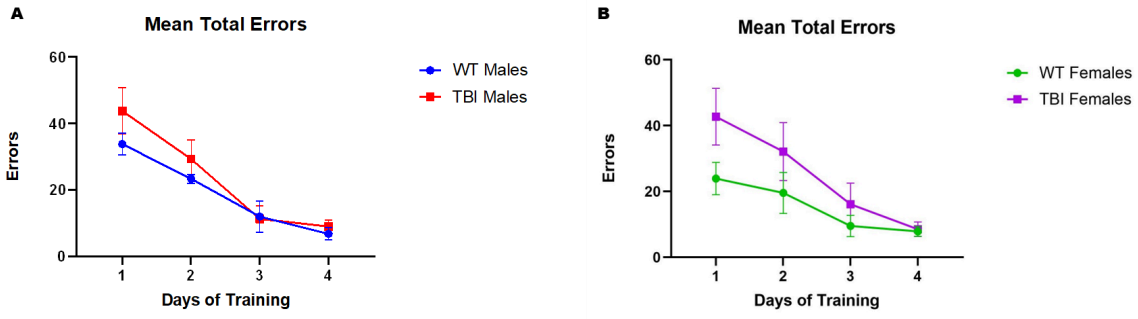

Figure 5. Total Errors Made During Barnes Maze Training. (A) Total number of errors made by WT and TBI males. No significant differences were seen (*p>0.05*). (B) Total number of errors made by WT and TBI females. No significant differences observed (*p>0.05)*. Values are mean ± SEM. Significance determined by two-way ANOVA with Tukey HSD post-test.

3.3.3 Probe Test:

The probe trial showed that TBI females spent significantly less time in the goal zone than WT females (*p=0.0358,* Fig. 6). Additionally, no significant differences were seen between TBI and WT males.

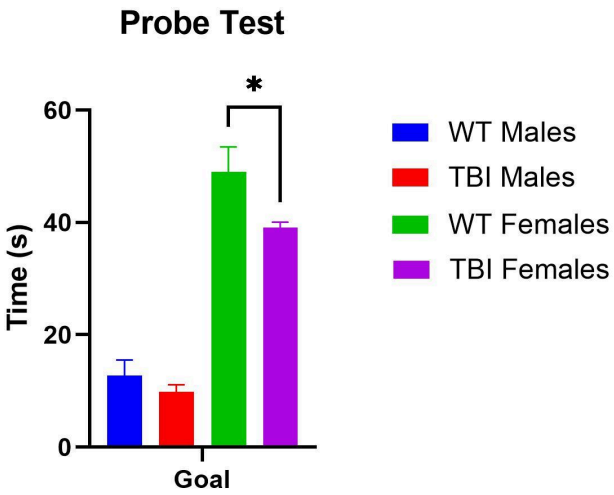

Figure 6. Time Spent Exploring the Goal Zone During the Probe Test. TBI females spent significantly less time exploring the goal zone than WT females (* p=0.0358). Values are mean ± SEM. Significance determined by two-way ANOVA with Tukey HSD post-test.

3.3.4 Spatial Search Strategies:

Spatial search strategies utilized during the Barnes maze were evaluated via the BUNS classification tool (see Materials and Methods).[26] On the first day of training, TBI and WT males utilized random search and serial search strategies (Fig. 7A and 7B). Additionally, TBI and WT females utilized random and serial strategies as well as more direct search strategies on day 1 of training (Fig. 7C and 7D). By the fourth day of training, these strategies shifted from a majority random and serial search to more direct strategies for all groups. Interestingly, TBI and WT males used direct strategies approximately 60-75% of the time, whereas TBI and WT females used direct strategies only ~50% of the time.

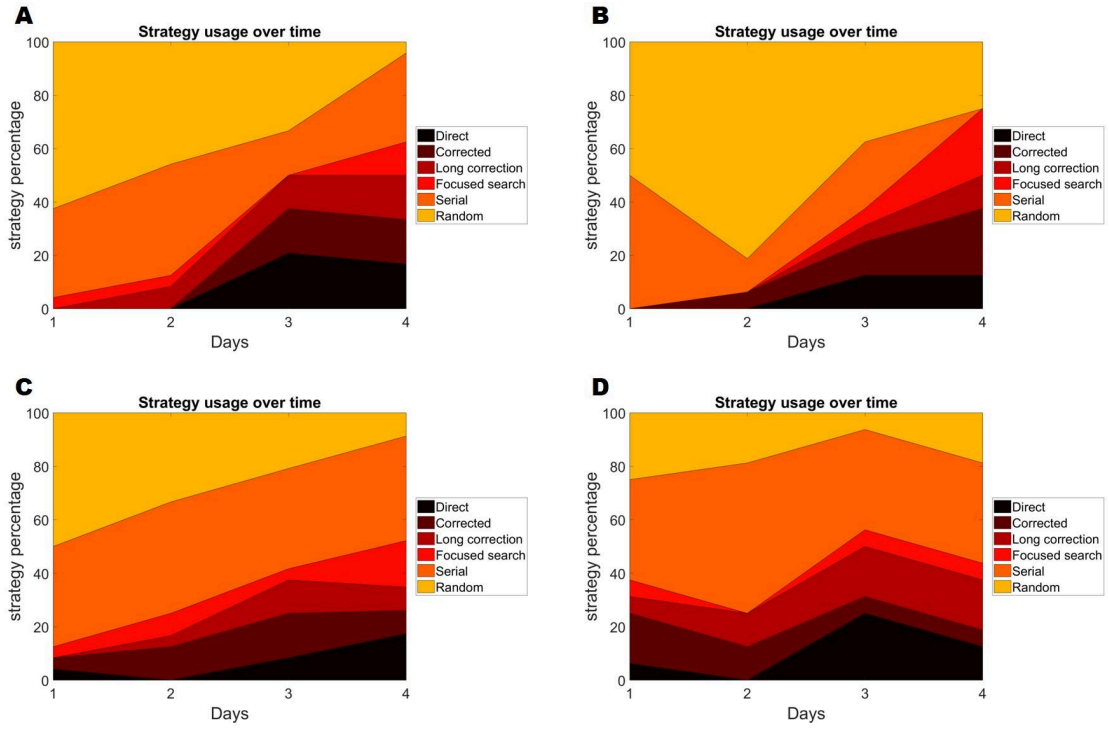

Figure 7. Barnes Maze Spatial Search Strategies (Training) A: TBI males. B: WT males. C: TBI females. D: WT females. All figures display the percentage of spatial search strategies utilized over the four days of Barnes maze training.

During the probe test, TBI males utilized serial-random, serial, and focused search strategies (Fig. 8A). WT males and females both utilized serial random and focused search strategies (Fig. 8B and 8D). TBI females, however, only used the serial-random search strategy during the probe test (Fig. 8C).

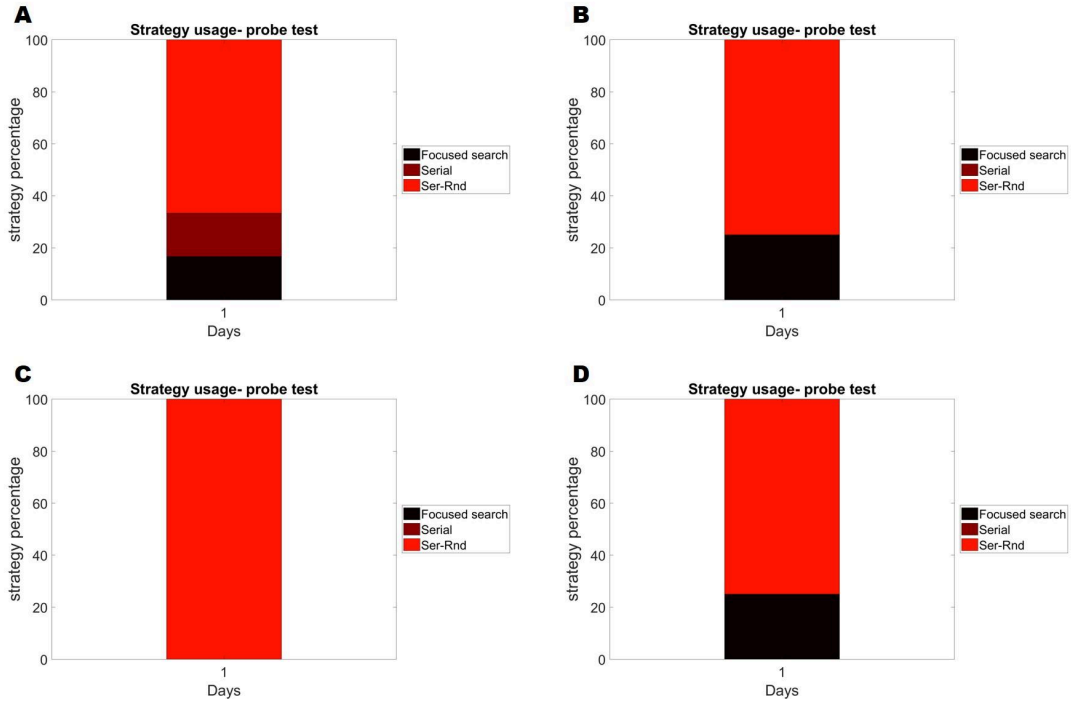

Figure 8. Barnes Maze Spatial Search Strategies (Probe Test). A: TBI males. B: WT males. C: TBI females. D: WT females. All figures display the percentage of spatial search strategies utilized during the probe trial.

3.4 Fear Conditioning:

Associative learning and memory formation were evaluated utilizing delay fear conditioning (see materials and methods). During the conditioning phase, all mice performed similarly with no significant differences in percent time spent

freezing (WT males: 34.1±8.8%, TBI males: 31.9±8%, WT females: 36.6±6.1%, TBI females: 28.6±3.3%; Fig. 9A). Context-dependent memory testing revealed that TBI mice spent slightly more time freezing than WT mice, though these differences were not statistically significant (WT males: 19.9±8.6%, TBI males: 32.7±8.6%, WT females: 12.6±5.6%, TBI females: 23.9±7.5%; Fig. 9B). Similarly, no significant differences were seen between TBI and WT mice during cued memory testing (WT males: 58.4±9.6%, TBI males: 58.9±6.7%, WT females: 63.4±2.1%, TBI females: 62.4±5.8%; Fig. 9C). Though not significant, this data illustrates a trend towards significance. To determine the approximate sample size necessary for statistical significance, a power analysis was conducted. To achieve significance (power = 0.8), a total sample size of 180 animals (45 animals per group) would be necessary (Fig. 9D).

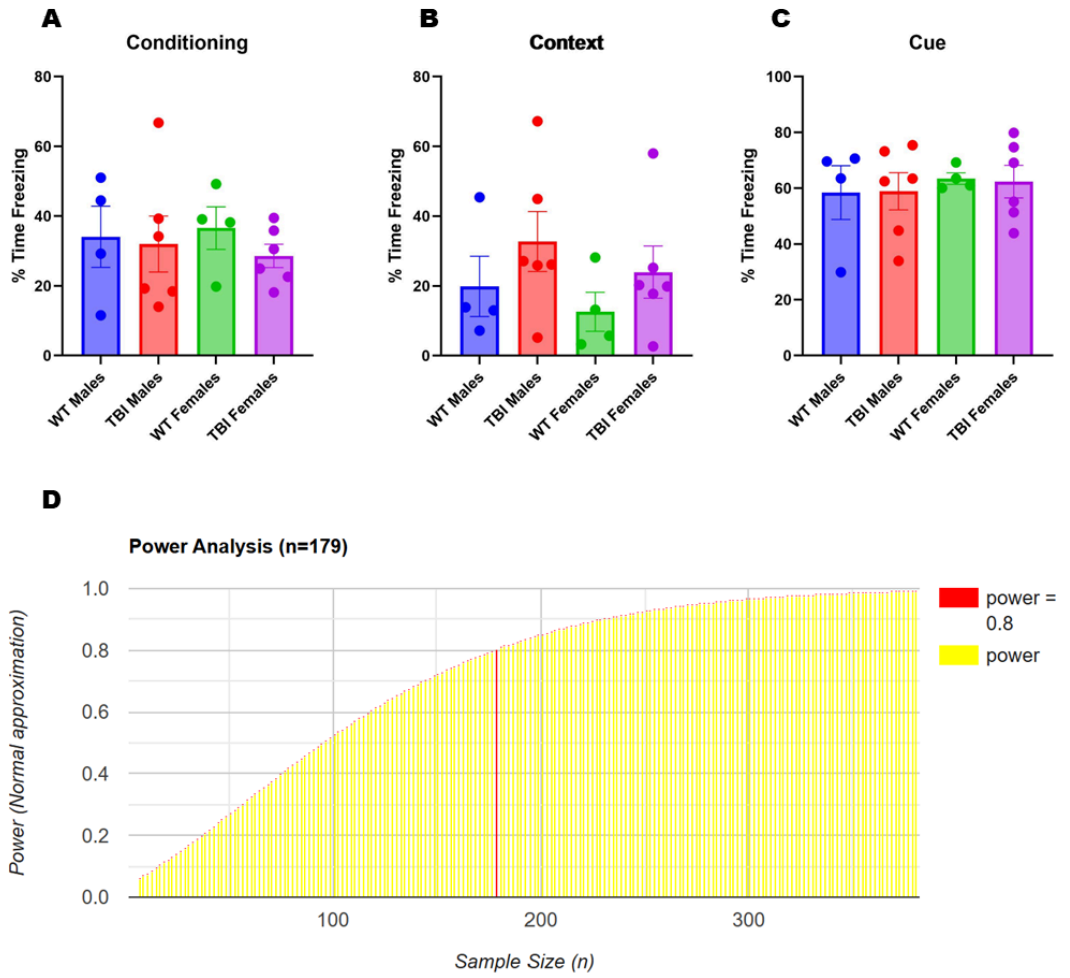

Figure 9. Fear Conditioning Results. (A) Percent time spent freezing during the conditioning phase. (B) Percent time spent freezing during the context memory test. (C) Percent time spent freezing during the cued memory test. (D) Power analysis to determine the approximate sample size needed for significance (n = 45/group, 180 total mice). No significant differences were seen between groups. Values are mean ± SEM. Statistical analysis by one-way ANOVA with Tukey HSD post-test.

3.5 Lesion Volume Analysis and Mapping:

Total TBI lesion volume was evaluated using 3D ultrasound and 3D Slicer (see materials and methods). Lesion volume analysis revealed no significant differences between TBI male and female mice (TBI males: 2.7±0.6 mm^3, TBI

females: 2.4±0.9 mm^3; Fig. 10.1). 3D ultrasound scans were then mapped to the Allen Brain Reference Atlas to precisely identify brain regions affected by traumatic brain injury (TBI) and to quantify the volume of tissue lost in each region. By comparing TBI lesions to the Allen Brain Atlas, we observed that the primary somatosensory cortex, primary motor cortex, caudoputamen, and anterior brain regions were most consistently impacted (Fig. 10.2). Notably, the primary somatosensory area exhibited the greatest volume loss in both male and female TBI mice, with an average of 2.08 mm^3 lost in males and 1.13 mm^3 in females (Fig. 10.3). This difference was statistically significant, suggesting a sex-specific vulnerability in this region (*$p<0.001$)*. In contrast, no significant sex differences in volume loss were observed in the other affected brain regions, including the primary motor area (0.22mm^3 in males vs. 0.27mm^3 in females), caudoputamen (0.18mm^3 in males vs 0.17mm^3 in females), and anterior area (0.22mm^3 in males vs. 0.14mm^3 in females).

Since male TBI mice exhibited the most pronounced volume loss in the primary somatosensory area, a simple linear regression was performed to determine whether there was a significant correlation between the number of total foot faults at 20 DPI and the volume of tissue lost specifically within the primary somatosensory area. The simple linear regression revealed a weakly positive, insignificant correlation between total foot faults and SSp volume loss (R^2=0.3916, *$p=0.1839$,* Fig. 10.4). Though not significant, the weak positive correlation suggests a trend towards significance. Thus, a power analysis was

conducted to determine the approximate sample size necessary for statistical significance. To achieve significance (power = 0.8), a total sample size of 54 animals would be necessary (Fig. 10.5).

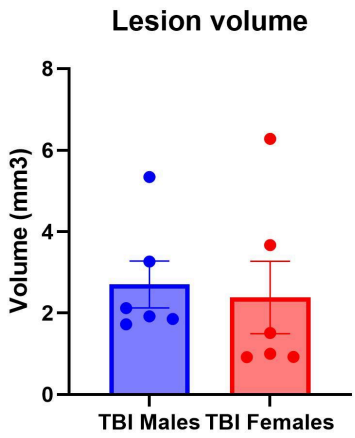

Figure 10.1 Lesion Volumes of TBI Male and Female Mice. No significant differences were seen between groups. Values are mean ± SEM. Significance determined by two-tailed unpaired t-test.

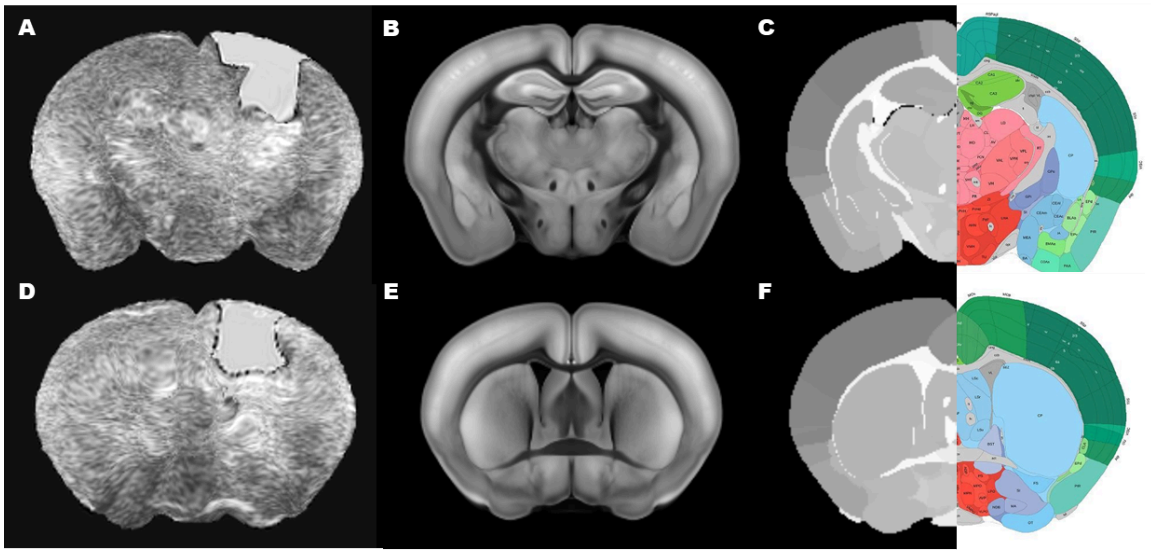

Figure 10.2 Side by Side Comparison of Normalized Ultrasound Scan and Allen Brain Annotation Atlas. (A&D) Normalized scan of TBI lesion and brain. (B&E) Normalized scan merged with Allen Brain Atlas. (C&F) Normalized scan merged with Allen Brain Annotation Atlas. A-C shows representative TBI male scans while D-F shows TBI female scans.

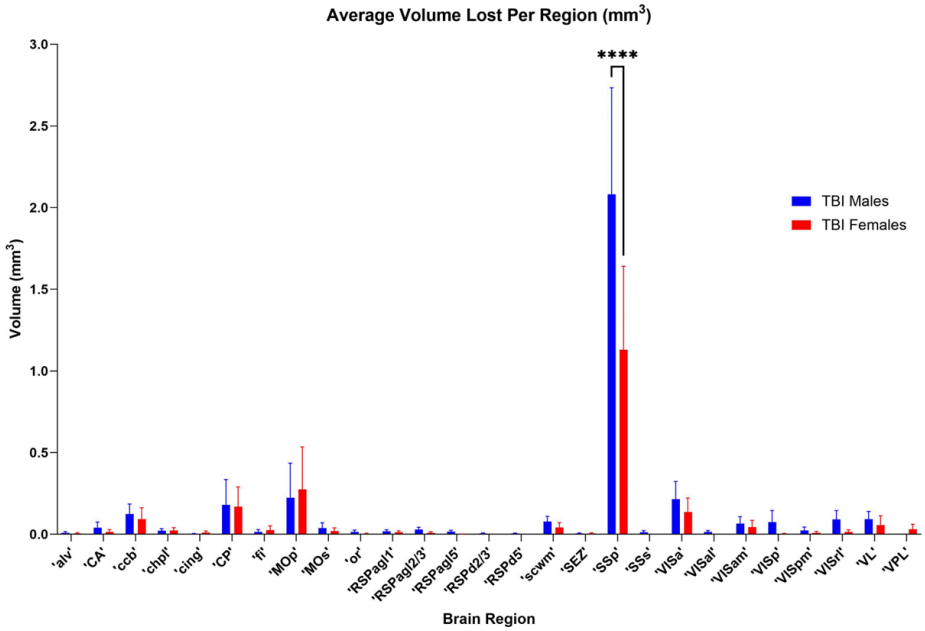

Figure 10.3. Average Volume Missing Per Region for Male and Female Mice. Quantified through Ultrasound Estimation. Regions with average loss below .005 were excluded. TBI males had significantly more volume lost in the SSp region compared to TBI females (*****p<0.001)*. Acronyms listed in Table 1.

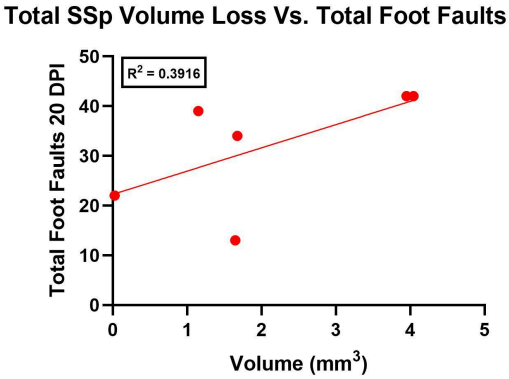

Figure 10.4. Simple Linear Regression. Simple linear regression analysis comparing total foot faults at 20 DPI to the total volume loss of the primary somatosensory region of TBI males. Each point represents an individual subject. A weak, nonsignificant positive correlation was observed, suggesting a trend towards significance (R^2=0.3916, *p=0.1839)*.

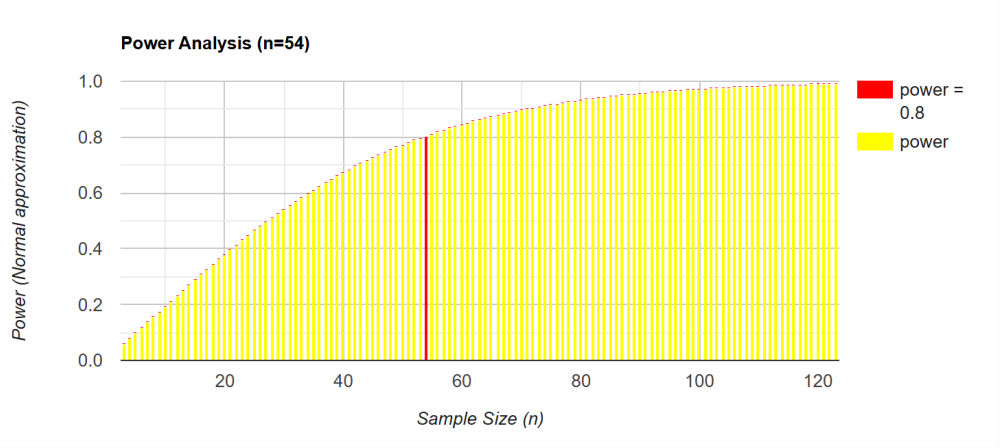

Figure 10.5. Power Analysis. Power analysis to determine the approximate sample size needed for a significant positive correlation between total foot faults and volume loss (n = 54/group).

Acronym	**Name**
alv	Alveus
CA	Ammon's Horn
ccb	Corpus Callosum, body
chpl	Choroid Plexus
cing	Cingulum Bundle
CP	Caudoputamen
fi	Fimbria
MOp	Primary Motor Area
MOs	Secondary Motor Area
or	Oriens Layer, Hippocampus
RSPagl1	Retrosplenial Area, lateral agranular part, layer 1
RSPagl2/3	Retrosplenial Area, lateral agranular part, layer 2/3
RSPagl5	Retrosplenial Area, lateral agranular part, layer 5
RSPd2/3	Retrosplenial Area, dorsal part, layer 2/3
RSPd5	Retrosplenial Area, dorsal part, layer 5
scwm	Supra-Callosal Cerebral White Matter
SEZ	Subependymal Zone
SSp	Primary Somatosensory Area
SSs	Supplemental Somatosensory Area
VISa	Anterior Area
VISal	Anterolateral Visual Area
VISam	Anteromedial Visual Area
VISp	Primary Visual Area
VISpm	Posteromedial Visual Area

VISrl	Rostrolateral Visual Area
VL	Lateral Ventricle
VPL	Ventral Posterolateral Nucleus of the Thalamus

Table 1. List of Allen Brain Atlas Acronyms.

3.6 Histology:

Histological changes associated with moderate TBI in the anterior cortical site of injury were evaluated via immunofluorescence staining of Iba-1 and GFAP, followed by the quantification of astrocytic and microglial activation in the ipsilateral and contralateral cortices and hippocampus (see materials and methods). Phenotypic analysis revealed that both male and female TBI mice exhibited morphological features characteristic of chronic microglial and astrocytic activation, including increased soma size, cell hypertrophy, and process retraction. Conversely, male and female WT mice displayed morphological features characteristic of healthy/resting glial cells, including small cell somas with thin, highly-branched cell processes (Fig. 11).

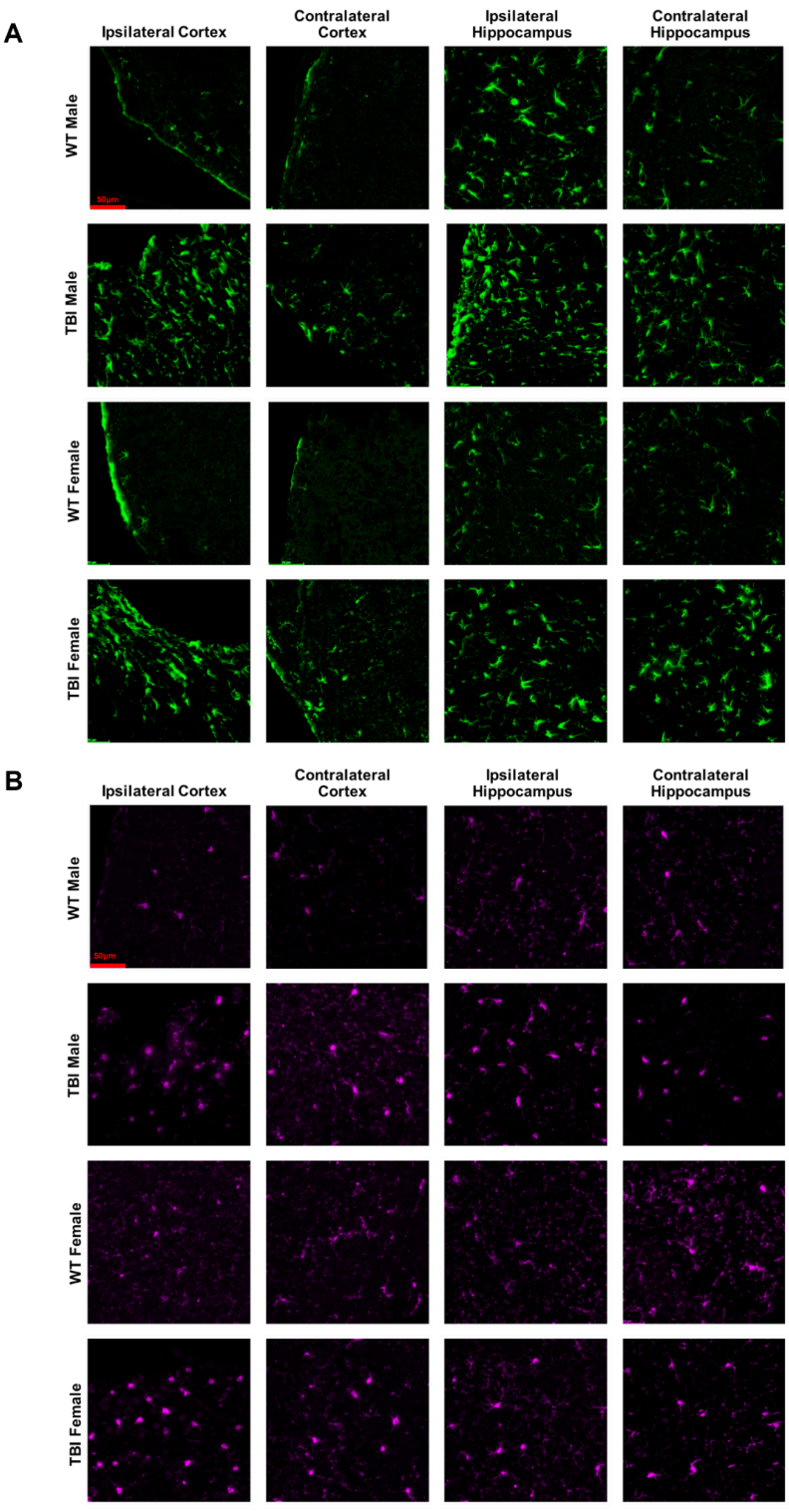

Figure 11. Representative Images of GFAP and Iba-1 Staining. (A) GFAP+ astrocytes. (B) Iba-1+ microglia. Scale bars represent 50μM. Images taken at 40X magnification.

In addition to these morphological differences, quantitative analysis showed significantly higher percentages of activated astrocytes and microglia in the ipsilateral and contralateral cortices of both male and female TBI mice as compared to their WT counterparts (*p<0.015*, Fig. 12A and 12B). Similar trends were seen for the ipsilateral and contralateral hippocampi of TBI and WT mice (*p≤0.0006*, Fig. 12A and 12B).

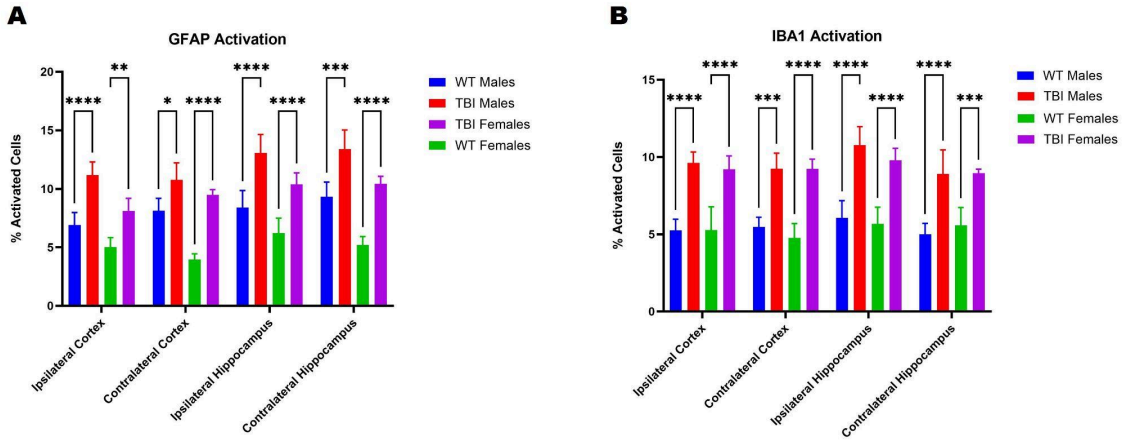

Figure 12. Microglial and Astrocytic Activation. (A) Percentage of activated GFAP+ cells in the ipsilateral and contralateral cortices and hippocampi. (B) Percentage of activated Iba1+ cells in the ipsilateral and contralateral cortices and hippocampi. Values are mean ± SEM. Significance determined by two-way ANOVA with Tukey HSD post-test (* p=0.0138, ** p=0.0031, *** = p≤0.0006, ****= p≤0.0001).

Chapter 4: Discussion

4.1 Overview:

In this study, the behavioral and histological impact of moderate anterior CCI induced TBI in mice was interrogated. Behavior testing revealed that moderate TBI of the anterior sensory-motor cortices induces sustained deficits in sensorimotor function and spatial memory, but not spatial learning acquisition or fear response. Additionally, we show that over time, this TBI coordinate induces widespread, chronic activation of microglia and astrocytes.

4.2 Behavior Testing:

Deficits in motor coordination and cognition are commonly seen in human TBI patients following injury.[26,29] Therefore, many preclinical studies employ behavioral tasks like the beam walk, rotarod, Barnes maze, and fear conditioning to assess sensorimotor and cognitive dysfunction in animal models of TBI.

4.2.1 Beam Walk and Rotarod:

In agreement with prior literature, our beam walk results showed significantly increased foot faults in TBI mice as compared to WT mice, which persisted through 27 DPI (Fig. 2).[30-32] Additionally, the rotarod task in this study illustrated that TBI mice spent significantly less time on the apparatus than WT animals at 1 DPI, as well as 6 DPI for females only (Fig. 3A and 3B). These results are consistent with previous reports that rotarod performance of TBI mice return to sham/WT levels at 7 DPI.[30,33] Overall, this data suggests that moderate TBI of the anterior sensory-motor cortex induces significant deficits in fine motor

coordination and individual limb function, as well as mild deficits in gross motor coordination.

4.2.2 Barnes Maze:

The Barnes maze was conducted to assess spatial learning and memory in TBI and WT mice. Here, both groups made similar amounts of total errors across the four days of training. Additionally, both groups showed a shift from nonspatial (serial/random) search strategies to focused/direct search strategies from day 1 to day 4 of training. These observations are inconsistent with those of prior studies, which report that TBI animals make more total errors and predominantly use serial and/or random spatial search strategies.[31,34-36] In line with prior literature, however, we observed that TBI Females exhibited significantly longer escape latencies than WT females on day 1 of training, as well as a significant group x time interaction.[31] Additionally, we found that TBI females spent significantly less time exploring the goal zone than WT females during the probe test.[37] Spatial search strategy analysis further showed that female TBI mice utilized serial/random search patterns while WT females used a mix of serial/random and focused search strategies. These findings suggest that TBI at this anterior coordinate leads to significant and lasting deficits in long-term spatial learning and memory retention in female mice. Surprisingly, the WT control male mice did not complete the Barnes maze tasks as expected. It is uncertain as to why the WT males did not perform as expected, therefore, we cannot draw any

conclusions on the effect of anterior TBI on spatial learning and memory capabilities in male mice.

4.2.3 Fear Conditioning:

Alongside beam walk, rotarod, and the Barnes maze, delay fear conditioning was conducted to evaluate the fear response of TBI and WT mice. In agreement with prior literature, we found no statistically significant differences in the percentage of time spent freezing during the conditioning phase, context memory test, or cued memory test between TBI and WT mice.[38] We did, however, notice a trend towards significance during the context-dependent memory test. Through a power calculation, we discovered that a sample size of n=145 animals (45 animals/group) would be necessary to achieve significance.

While this overall lack of significance is likely due to the absence of amygdalar damage at the anterior cortical injury location, it's plausible that the trend towards significance — expected to achieve significance with a larger sample size — may be driven by damage to other brain regions known to contribute to fear learning and memory. Previous literature suggests that the amygdala, hippocampus, anterior cingulate cortex, striatum, and retrosplenial cortex function together as a neuroconnective circuit involved in fear learning and memory formation.[38-41] Though our TBI model did not damage the amygdala, we observed injury to the caudoputamen, cingulum bundle, and adjacent anterior cortical regions, including the retrosplenial and visual association areas: regions implicated in this broader fear circuitry.

Overall, these findings suggest that the anterior cortical injury coordinate employed in this study is not sufficient to disrupt amygdala-dependent fear learning and memory with the sample size utilized in this study. However, if we wanted to allocate the time, resources, and budget to accommodate a larger large sample size, it is likely we would see significant differences in the percentage of time spent freezing between groups.

4.3 Lesion Volume Analysis:

Lesion volume was quantified using 3D ultrasound imaging, revealing consistent focal damage across TBI animals, with mean lesion volumes ranging from 2.4-2.7mm^3. These values align with prior moderate CCI models employing comparable depth and impact velocity parameters.[42,43] Importantly, lesion localization was not diffuse but topographically selective. When mapped to the Allen Brain Atlas, the lesion consistently encompassed the primary somatosensory cortex (SSp), primary motor cortex (MOp), caudoputamen (CP), and adjacent anterior cortical regions, including retrosplenial and visual association areas. The most substantial volume loss occurred in the primary somatosensory cortex, with significantly greater tissue damage observed in male mice compared to females. This regional specificity is functionally meaningful, as the SSp and MOp are involved in sensorimotor integration, proprioception, and fine motor control.[44]

Behavioral assessments corroborated this anatomical pattern, with TBI animals exhibiting persistent deficits in motor coordination on the beam walk and

reduced balance on the rotarod. These impairments were especially pronounced in TBI male mice, aligning with their increased lesion burden. Interestingly, a simple linear regression revealed a weakly positive but non-significant relationship between total foot faults at 20 DPI and SSp tissue damage in TBI male mice. However, a power analysis indicated that a significant positive correlation would be detectable with a sample size of 54 mice, suggesting a meaningful association between lesion burden and beam walk performance. Conversely, deep limbic structures such as the amygdala were spared from structural damage, which is consistent with the preserved performance in fear learning and memory.

Thus these data support the premise that region-specific tissue loss drives selective behavioral impairments, reinforcing the need for anatomically resolved lesion analysis in TBI research. Moreover, the sex-specific variation in lesion magnitude within the somatosensory cortex may underlie the differential cognitive recovery observed between male and female mice, despite equivalent injury parameters.

4.4 Histology:

Immunofluorescence analysis revealed robust microglial and astrocytic activation bilaterally, with dense gliosis in the lesion core that extends into the contralateral cortex and both hippocampus. This pattern reflects secondary injury mechanisms such as excitotoxicity, danger-associated molecular pattern (DAMP) release, and glial priming, that drive diffuse neuroinflammation even from a focal primary

insult.[45] These findings align with prior literature, in which bilateral hippocampal microglial activation following unilateral CCI was observed, thus suggesting that interhemispheric propagation of inflammatory cascades are a hallmark of moderate TBI.[46] Interestingly, the amygdala showed only low-grade gliosis, suggesting that deep limbic structures remain largely protected in this anterior model of CCI. These observations contrast with posterior or ventrolateral TBI models, where direct or indirect involvement of the amygdala leads to pronounced astrogliosis and disrupted fear learning.[47]

Although the overall pattern of glial activation seen in this study did not differ markedly between sexes, prior reports have documented sex-dependent differences in the timing and resolution of neuroinflammatory responses. Specifically, prior literature suggests that male mice tend to show an earlier peak in microglial activity, whereas female mice exhibit a more prolonged inflammatory phase.[48,49] In this context, our observation of similar lesion volumes but worse memory performance in female mice could reflect underlying differences in neuroimmune dynamics rather than structural damage per se.

4.5 Conclusion:

This study establishes the anterior CCI model as a robust, reproducible and anatomically informative platform for investigating moderate traumatic brain injury in mice. Lesion mapping revealed consistent involvement of sensorimotor and associative cortices, with the primary somatosensory cortex showing the greatest volume loss, particularly in male mice. This region-specific structural damage

corresponded with marked impairments in motor coordination and long-term spatial memory, while fear-related behaviors remained intact, likely due to anatomical sparing of the amygdala. Histologically, focal injury initiated a bilateral neuroinflammatory cascade, evidenced by widespread microglial and astrocytic activation extending into both cortices and the hippocampus. These findings reflect secondary injury propagation beyond the lesion core, a hallmark of moderate TBI. Importantly, behavioral impairments closely mirrored the anatomical regions impacted by both primary damage and secondary gliosis, emphasizing the translational relevance of this model. The anterior CCI model presented here enables precise correlation of lesion topography with functional outcome and glial pathology. It provides a valuable framework for examining region-dependent vulnerability, sex-specific injury responses, and for evaluating candidate therapies targeting structural and inflammatory sequelae of moderate TBI.

Chapter 5: Bibliography

1. Haarbauer-Krupa, J., Pugh, M. J., Prager, E. M., Harmon, N., Wolfe, J., & Yaffe, K. (2021). Epidemiology of Chronic Effects of Traumatic Brain Injury. *Journal of Neurotrauma*, *38*(23), 3235–3247. https://doi.org/10.1089/neu.2021.0062

2. Vadan and Ilut. (2022). *Estimating the global incidence of TBI*. Academy for Multidisciplinary Neurotraumatology. https://brain-amn.org/global-incidence-of-tbi/

3. Jain, S., & Iverson, L. M. (2025). Glasgow Coma Scale. In *StatPearls*. StatPearls Publishing. http://www.ncbi.nlm.nih.gov/books/NBK513298/

4. Siebold, L., Obenaus, A., & Goyal, R. (2018). Criteria to define mild, moderate, and severe traumatic brain injury in the mouse controlled cortical impact model. *Experimental Neurology*, *310*, 48–57. https://doi.org/10.1016/j.expneurol.2018.07.004

5. Mckee, A. C., & Daneshvar, D. H. (2015). The neuropathology of traumatic brain injury. *Handbook of Clinical Neurology*, *127*, 45–66. https://doi.org/10.1016/B978-0-444-52892-6.00004-0

6. Xiong, Y., Mahmood, A., & Chopp, M. (2013). Animal models of traumatic brain injury. *Nature Reviews. Neuroscience*, *14*(2), 128–142. https://doi.org/10.1038/nrn3407

7. Mcallister, T. W. (2008). Neurobehavioral sequelae of traumatic brain injury: Evaluation and management. *World Psychiatry*, *7*(1), 3–10. https://www.ncbi.nlm.nih.gov/pmc/articles/PMC2327235/

8. National Center for Injury Prevention and Control. (n.d.). *Moderate to Severe Traumatic Brain Injury is a Lifelong Condition*.

9. Amlerova, Z., Chmelova, M., Anderova, M., & Vargova, L. (2024). Reactive gliosis in traumatic brain injury: A comprehensive review. *Frontiers in Cellular Neuroscience*, *18*, 1335849. https://doi.org/10.3389/fncel.2024.1335849

10. Dodd, W. S., Panther, E. J., Pierre, K., Hernandez, J. S., Patel, D., & Lucke-Wold, B. (2022). Traumatic Brain Injury and Secondary Neurodegenerative Disease. *Trauma Care*, *2*(4), Article 4. https://doi.org/10.3390/traumacare2040042

11. Vidal-Itriago, A., Radford, R. A. W., Aramideh, J. A., Maurel, C., Scherer, N. M., Don, E. K., Lee, A., Chung, R. S., Graeber, M. B., & Morsch, M. (2022). Microglia morphophysiological diversity and its implications for the CNS. *Frontiers in Immunology*, *13*, 997786. https://doi.org/10.3389/fimmu.2022.997786

12. Garland, E. F., Hartnell, I. J., & Boche, D. (2022). Microglia and Astrocyte Function and Communication: What Do We Know in Humans? *Frontiers in Neuroscience*, *16*. https://doi.org/10.3389/fnins.2022.824888

13. Var, S. R., Shetty, A. V., Grande, A. W., Low, W. C., & Cheeran, M. C. (2021). Microglia and Macrophages in Neuroprotection, Neurogenesis, and Emerging Therapies for Stroke. *Cells*, *10*(12), 3555. https://doi.org/10.3390/cells10123555

14. Donat, C. K., Scott, G., Gentleman, S. M., & Sastre, M. (2017). Microglial Activation in Traumatic Brain Injury. *Frontiers in Aging Neuroscience*, *9*, 208. https://doi.org/10.3389/fnagi.2017.00208

15. Loane, D. J., & Kumar, A. (2016). Microglia in the TBI Brain: The Good, The Bad, And The Dysregulated. *Experimental Neurology*, *275*(0 3), 316–327. https://doi.org/10.1016/j.expneurol.2015.08.018

16. Zhang, L., Wang, Y., Liu, T., Mao, Y., & Peng, B. (2023). Novel Microglia-based Therapeutic Approaches to Neurodegenerative Disorders. *Neuroscience Bulletin*, *39*(3), 491–502. https://doi.org/10.1007/s12264-022-01013-6

17. Dinet, V., Petry, K. G., & Badaut, J. (2019). Brain-Immune Interactions and Neuroinflammation After Traumatic Brain Injury. *Frontiers in Neuroscience*, *13*, 1178. https://doi.org/10.3389/fnins.2019.01178

18. Faden, A. I., Barrett, J. P., Stoica, B. A., & Henry, R. J. (2021). Bidirectional Brain-Systemic Interactions and Outcomes After TBI. *Trends in Neurosciences*, *44*(5), 406–418. https://doi.org/10.1016/j.tins.2020.12.004

19. Franklin, H., Clarke, B. E., & Patani, R. (2021). Astrocytes and microglia in neurodegenerative diseases: Lessons from human *in vitro* models. *Progress in Neurobiology*, *200*, 101973. https://doi.org/10.1016/j.pneurobio.2020.101973

20. Agarwal et al. (n.d.). *Traumatic Brain Injury – Causes, Symptoms and Treatments*. Retrieved June 20, 2023, from https://www.aans.org/

21. Leconte, C., Benedetto, C., Lentini, F., Simon, K., Ouaazizi, C., Taib, T., Cho, A., Plotkine, M., Mongeau, R., Marchand-Leroux, C., & Besson, V. C. (2020). Histological and Behavioral Evaluation after Traumatic Brain Injury in Mice: A Ten Months Follow-Up Study. *Journal of Neurotrauma*, *37*(11), 1342–1357. https://doi.org/10.1089/neu.2019.6679

22. Lerouet, D., Marchand‐Leroux, C., & Besson, V. C. (2021). Neuropharmacology in traumatic brain injury: From preclinical to clinical neuroprotection? *Fundamental & Clinical Pharmacology*, *35*(3), 524–538. https://doi.org/10.1111/fcp.12656

23. Hoogenboom, W. S., Branch, C. A., & Lipton, M. L. (2019). Animal models of closed-skull, repetitive mild traumatic brain injury. *Pharmacology & Therapeutics*, *198*, 109–122. https://doi.org/10.1016/j.pharmthera.2019.02.016

24. Fujimoto, S. T., Longhi, L., Saatman, K. E., & McIntosh, T. K. (2004). Motor and cognitive function evaluation following experimental traumatic brain injury. *Neuroscience*

& Biobehavioral Reviews, *28*(4), 365–378. https://doi.org/10.1016/j.neubiorev.2004.06.002

25. Washington, P. M., Forcelli, P. A., Wilkins, T., Zapple, D. N., Parsadanian, M., & Burns, M. P. (2012). The effect of injury severity on behavior: A phenotypic study of cognitive and emotional deficits after mild, moderate, and severe controlled cortical impact injury in mice. *Journal of Neurotrauma*, *29*(13), 2283–2296. https://doi.org/10.1089/neu.2012.2456

26. Illouz, T., Madar, R., Clague, C., Griffioen, K. J., Louzoun, Y., & Okun, E. (2016). Unbiased classification of spatial strategies in the Barnes maze. *Bioinformatics*, *32*(21), 3314–3320. https://doi.org/10.1093/bioinformatics/btw376

27. Fedorov, A., Beichel, R., Kalpathy-Cramer, J., Finet, J., Fillion-Robin, J.-C., Pujol, S., Bauer, C., Jennings, D., Fennessy, F., Sonka, M., Buatti, J., Aylward, S., Miller, J. V., Pieper, S., & Kikinis, R. (2012). 3D Slicer as an image computing platform for the Quantitative Imaging Network. *Magnetic Resonance Imaging*, *30*(9), 1323–1341. https://doi.org/10.1016/j.mri.2012.05.001

28. Bankhead, P., Loughrey, M. B., Fernández, J. A., Dombrowski, Y., McArt, D. G., Dunne, P. D., McQuaid, S., Gray, R. T., Murray, L. J., Coleman, H. G., James, J. A., Salto-Tellez, M., & Hamilton, P. W. (2017). QuPath: Open source software for digital pathology image analysis. *Scientific Reports*, *7*(1), 16878. https://doi.org/10.1038/s41598-017-17204-5

29. Whiting, M. D., Baranova, A. I., & Hamm, R. J. (2006). Cognitive Impairment following Traumatic Brain Injury. In E. D. Levin & J. J. Buccafusco (Eds.), *Animal Models of Cognitive Impairment*. CRC Press/Taylor & Francis. http://www.ncbi.nlm.nih.gov/books/NBK2521/

30. Fox, G. B., Fan, L., Levasseur, R. A., & Faden, A. I. (1998). Sustained sensory/motor and cognitive deficits with neuronal apoptosis following controlled cortical impact brain injury in the mouse. *Journal of Neurotrauma*, *15*(8), 599–614. https://doi.org/10.1089/neu.1998.15.599

31. Fox, G. B., Fan, L., LeVasseur, R. A., & Faden, A. I. (1998). Effect of traumatic brain injury on mouse spatial and nonspatial learning in the Barnes circular maze. *Journal of Neurotrauma*, *15*(12), 1037–1046. https://doi.org/10.1089/neu.1998.15.1037

32. Henry, R. J., Meadows, V. E., Stoica, B. A., Faden, A. I., & Loane, D. J. (2020). Longitudinal Assessment of Sensorimotor Function after Controlled Cortical Impact in Mice: Comparison of Beamwalk, Rotarod, and Automated Gait Analysis Tests. *Journal of Neurotrauma*, *37*(24), 2709–2717. https://doi.org/10.1089/neu.2020.7139

33. Tucker, L. B., Fu, A. H., & McCabe, J. T. (2016). Performance of Male and Female C57BL/6J Mice on Motor and Cognitive Tasks Commonly Used in Pre-Clinical Traumatic Brain Injury Research. *Journal of Neurotrauma*, *33*(9), 880–894. https://doi.org/10.1089/neu.2015.3977

34. Gawel, K., Gibula, E., Marszalek-Grabska, M., Filarowska, J., & Kotlinska, J. H. (2019). Assessment of spatial learning and memory in the Barnes maze task in rodents—Methodological consideration. *Naunyn-Schmiedeberg's Archives of Pharmacology*, *392*(1), 1–18. https://doi.org/10.1007/s00210-018-1589-y

35. Gee, C. C., Steffen, R., & Kievit, F. M. (2023). An updated Barnes maze protocol for assessing the outcome of controlled cortical impact mouse models of traumatic brain injury. *Journal of Neuroscience Methods*, *392*, 109866. https://doi.org/10.1016/j.jneumeth.2023.109866

36. Rodríguez Peris, L., Scheuber, M. I., Shan, H., Braun, M., & Schwab, M. E. (2024). Barnes maze test for spatial memory: A new, sensitive scoring system for mouse search strategies. *Behavioural Brain Research*, *458*, 114730. https://doi.org/10.1016/j.bbr.2023.114730

37. Newell, E. A., Todd, B. P., Luo, Z., Evans, L. P., Ferguson, P. J., & Bassuk, A. G. (2020). A Mouse Model for Juvenile, Lateral Fluid Percussion Brain Injury Reveals Sex-Dependent Differences in Neuroinflammation and Functional Recovery. *Journal of Neurotrauma*, *37*(4), 635–646. https://doi.org/10.1089/neu.2019.6675

38. Sierra-Mercado, D., McAllister, L. M., Lee, C. C. H., Milad, M. R., Eskandar, E. N., & Whalen, M. J. (2015). Controlled cortical impact before or after fear conditioning does not affect fear extinction in mice. *Brain Research*, *1606*, 133–141. https://doi.org/10.1016/j.brainres.2015.02.031

39. LeDoux, J. E. (2000). Emotion Circuits in the Brain. *Annual Review of Neuroscience*, *23*(Volume 23, 2000), 155–184. https://doi.org/10.1146/annurev.neuro.23.1.155

40. Greco, J. A., & Liberzon, I. (2016). Neuroimaging of Fear-Associated Learning. *Neuropsychopharmacology*, *41*(1), 320–334. https://doi.org/10.1038/npp.2015.255

41. Maren, S., Phan, K. L., & Liberzon, I. (2013). The contextual brain: Implications for fear conditioning, extinction and psychopathology. *Nature Reviews. Neuroscience*, *14*(6), 417–428. https://doi.org/10.1038/nrn3492

42. Clark, I. H., Natera, D., Grande, A. W., & Low, W. C. (2024). Ex vivo method for rapid quantification of post traumatic brain injury lesion volumes using ultrasound. *Journal of Neuroscience Methods*, *407*, 110140. https://doi.org/10.1016/j.jneumeth.2024.110140

43. Frank, D., Gruenbaum, B. F., Shelef, I., Zvenigorodsky, V., Benjamin, Y., Shapoval, O., Gal, R., Zlotnik, A., Melamed, I., & Boyko, M. (2021). A Novel Histological Technique to Assess Severity of Traumatic Brain Injury in Rodents: Comparisons to Neuroimaging and Neurological Outcomes. *Frontiers in Neuroscience*, *15*, 733115. https://doi.org/10.3389/fnins.2021.733115

44. Gale, D. J., Flanagan, J. R., & Gallivan, J. P. (2021). Human Somatosensory Cortex Is Modulated during Motor Planning. *The Journal of Neuroscience*, *41*(27), 5909–5922. https://doi.org/10.1523/JNEUROSCI.0342-21.2021

45. Burda, J. E., & Sofroniew, M. V. (2014). Reactive gliosis and the multicellular response to CNS damage and disease. *Neuron*, *81*(2), 229–248. https://doi.org/10.1016/j.neuron.2013.12.034

46. Caplan, H. W., Cardenas, F., Gudenkauf, F., Zelnick, P., Xue, H., Cox, C. S., & Bedi, S. S. (2020). Spatiotemporal Distribution of Microglia After Traumatic Brain Injury in Male Mice. *ASN Neuro*, *12*, 1759091420911770. https://doi.org/10.1177/1759091420911770

47. Palmer, C. P., Metheny, H. E., Elkind, J. A., & Cohen, A. S. (2016). Diminished amygdala activation and behavioral threat response following traumatic brain injury. *Experimental Neurology*, *277*, 215–226. https://doi.org/10.1016/j.expneurol.2016.01.004

48. Acaz-Fonseca, E., Duran, J. C., Carrero, P., Garcia-Segura, L. M., & Arevalo, M. A. (2015). Sex differences in glia reactivity after cortical brain injury. *Glia*, *63*(11), 1966–1981. https://doi.org/10.1002/glia.22867

49. Doran, S. J., Ritzel, R. M., Glaser, E. P., Henry, R. J., Faden, A. I., & Loane, D. J. (2019). Sex Differences in Acute Neuroinflammation after Experimental Traumatic Brain

Injury Are Mediated by Infiltrating Myeloid Cells. *Journal of Neurotrauma*, *36*(7), 1040–1053. https://doi.org/10.1089/neu.2018.6019